

X-ray phase-sensitive microscope imaging with a grating interferometer:Theory and simulation

Jiecheng Yang(杨杰成), Peiping Zhu(朱佩平), Dong Liang(梁栋), Hairong Zheng(郑海荣), and Yongshuai Ge(葛永帅)

Citation: Chin. Phys. B, 2022, 31 (**9**): 098702. DOI: 10.1088/1674-1056/ac600e
Journal homepage: http://cpb.iphy.ac.cn; http://iopscience.iop.org/cpb

What follows is a list of articles you may be interested in

Analysis of period and visibility of dual phase grating interferometer

Jun Yang(杨君), Jian-Heng Huang(黄建衡), Yao-Hu Lei(雷耀虎), Jing-Biao Zheng(郑景标), Yu-Zheng Shan(单雨征), Da-Yu Guo(郭大育), and Jin-Chuan Guo(郭金川)
Chin. Phys. B, 2022, 31 (**5**): 058701. DOI: 10.1088/1674-1056/ac3a60

Quantitative coherence analysis of dual phase grating x-ray interferometry with source grating

Zhi-Li Wang(王志立), Rui-Cheng Zhou(周瑞成), Li-Ming Zhao(赵立明), Kun Ren(任坤), Wen Xu(徐文), Bo Liu(刘波), and Heng Chen(陈恒)
Chin. Phys. B, 2021, 30 (**2**): 028702. DOI: 10.1088/1674-1056/abb7fd

Single-shot grating-based x-ray differential phase contrast imaging with a modified analyzer grating

Chen-Xi Wei(卫晨希), Zhao Wu(吴朝), Faiz Wali, Wen-Bin Wei(魏文彬), Yuan Bao(鲍园), Rong-Hui Luo(骆荣辉), Lei Wang(王磊), Gang Liu(刘刚), Yang-Chao Tian(田扬超)
Chin. Phys. B, 2017, 26 (**10**): 108701. DOI: 10.1088/1674-1056/26/10/108701

Shifting curves based on the detector integration effect for x-ray phase contrast imaging

Jun Yang(杨君), Jin-Chuan Guo(郭金川), Yao-Hu Lei(雷耀虎), Ming-Hao Yi(易明皓), Li Chen(陈力)
Chin. Phys. B, 2017, 26 (**2**): 028701. DOI: 10.1088/1674-1056/26/2/028701

A new method for information retrieval in two-dimensional grating-based X-ray phase contrast imaging

Wang Zhi-Li, Gao Kun, Chen Jian, Ge Xin, Zhu Pei-Ping, Tian Yang-Chao, Wu Zi-Yu
Chin. Phys. B, 2012, 21 (**11**): 118703. DOI: 10.1088/1674-1056/21/11/118703

X-ray phase-sensitive microscope imaging with a grating interferometer: Theory and simulation

Jiecheng Yang(杨杰成)[1], Peiping Zhu(朱佩平)[2,3,†], Dong Liang(梁栋)[1,4], Hairong Zheng(郑海荣)[4], and Yongshuai Ge(葛永帅)[1,4,‡]

[1] *Research Center for Medical Artificial Intelligence, Shenzhen Institute of Advanced Technology, Chinese Academy of Sciences, Shenzhen* 518055, *China*
[2] *Platform of Advanced Photon Source Technology R&D, Laboratory of X-ray Optics and Technology, Beijing Synchrotron Radiation Facility, Institute of High Energy Physics, Chinese Academy of Sciences, Beijing*, 100049, *China*
[3] *Beijing Advanced Innovation Center for Imaging Theory and Technology, Capital Normal University, Beijing* 100048, *China*
[4] *Paul C Lauterbur Research Center for Biomedical Imaging, Shenzhen Institute of Advanced Technology, Chinese Academy of Sciences, Shenzhen* 518055, *China*

(Received 29 December 2021; revised manuscript received 10 March 2022; accepted manuscript online 23 March 2022)

A general theoretical framework is presented to explain the formation of the phase signal in an x-ray microscope integrated with a grating interferometer, which simultaneously enables the high spatial resolution imaging and the improved image contrast. By using this theory, several key parameters of phase contrast imaging can be predicted, for instance, the fringe visibility and period, and the conversion condition from the differential phase imaging (DPI) to the phase difference imaging (PDI). Additionally, numerical simulations are performed with certain x-ray optical components and imaging geometry. Comparison with the available experimental measurement [*Appl. Phys. Lett.* **113** 063105 (2018)] demonstrates the accuracy of this developed quantitative analysis method of x-ray phase-sensitive microscope imaging.

Keywords: x-ray phase contrast imaging, x-ray microscope, grating interferometer

PACS: 87.59.–e, 07.85.Tt, 07.60.Ly, 42.30.Rx **DOI:** 10.1088/1674-1056/ac600e

1. Introduction

The development of phase-sensitive x-ray imaging techniques over the last decades allows the measurement of the inner structure of weakly absorbing objects (e.g., soft tissue, and carbon materials) with high sensitivity, and dramatically complements the conventional absorption imaging. Among the various promising x-ray phase contrast imaging methods,[1–4] the grating-based x-ray Talbot and Talbot–Lau interferometers have been subject to increasing attention due to its compatibility with x-ray tube imaging systems. Many efforts[5–10] have been taken by integrating the Talbot (–Lau) interferometry with the full-field transmission x-ray microscope. One exciting progress is demonstrated by Takano *et al.*[10,11] on such a system to obtain superior phase information in comparison with the Zernike phase-contrast imaging approach. However, instead of generating the DPI images, such a combined x-ray microscope system produces the PDI images, which need to be post-processed via the iterative deconvolution method[12] or the maximum likelihood reconstruction method[13] to recover the phase information. Yashiro *et al.*[6,7] have provided pioneering theoretical explanations for such PDI phenomenon by exploiting the Talbot self-imaging effect.

In this work, a complete theoretical analysis for the imaging procedure of an x-ray microscope equipped with a grating interferometer is investigated. The theory has the capability to deal with various shaped source, and thus permits the explanations to other alternative interferometer designs, e.g., Lau typed interferometer. Additionally, the conversion condition from the PDI to the DPI, or vise versa, is quantitatively investigated with respect to the resolution limit of the imaging system. Finally, numerical simulations are performed to verify the consistency between the theoretical predictions and the previous experimental observations.[11]

2. Theoretical framework

The assumed x-ray microscope imaging system is depicted in Fig. 1. Herein, an arrayed x-ray source is considered. Every single point source on it is assumed to be spatially coherent and quasi-monochromatic. The object distance d_2 and the image distance (d_3+d_4) satisfy the thin lens equation $\frac{1}{d_2}+\frac{1}{d_3+d_4}=\frac{1}{f}$, in which f represents the focal length of the focusing device, e.g., the zone plate. The value of $M=(d_3+d_4)/d_2$ defines the magnification ratio of the system. In order to acquire the phase information besides the absorption signals, a $\pi/2$ phase grating is added between the zone plate and the detector.

In this study, the x-ray propagation is governed by Fresnel diffraction, which is a near-field approximation of the Kirchhoff–Fresnel diffraction for scalar waves. To simplify the derivations, the following analysis will be conducted in a one-dimensional (1D) case (along the x axis). The two-

†Corresponding author. E-mail: zhupp@ihep.ac.cn
‡Corresponding author. E-mail: ys.ge@siat.ac.cn

© 2022 Chinese Physical Society and IOP Publishing Ltd

dimensional (2D) results can be easily obtained upon this basis. With the paraxial approximation, the diffracted field $U_{\rm out}(x')$ at any distance d from the initial wave field $U_{\rm in}(x)$ can be expressed as

$$U_{\rm out}(x') = \mathscr{P}_d\left[U_{\rm in}(x)\right] = \frac{1}{\sqrt{{\rm i}\lambda d}}\int U_{\rm in}(x)\,{\rm e}^{{\rm i}k\left(d+\frac{(x'-x)^2}{2d}\right)}{\rm d}x, \quad (1)$$

where λ is the x-ray wavelength, and k $(=2\pi/\lambda)$ is the wave number. Such propagation of the initial wave field can be formally denoted by an action of the operator $\mathscr{P}$.

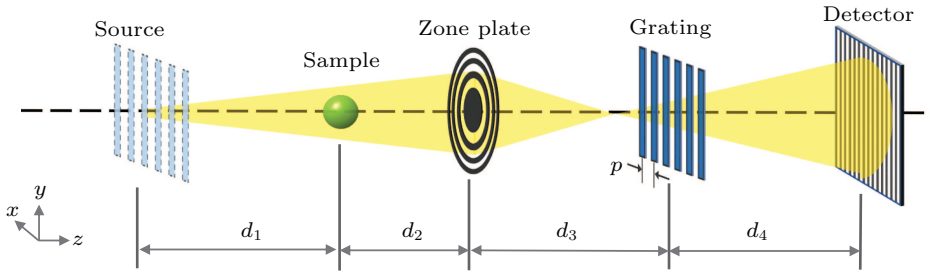


Fig. 1. Illustration of the x-ray phase contrast microscope system with an arrayed source and a $\pi/2$ phase grating.

By using Eq. (1), the scalar wave field $U_1(x_1)$ of a point source $\delta(x_0-\eta)$ (η denotes the off-axis distance) after propagating freely over a distance d_1 (before the sample) can be calculated as

$$U_1(x_1,\eta) = \mathscr{P}_{d_1}\left[\delta(x_0-\eta)\right] = \frac{1}{\sqrt{{\rm i}\lambda d_1}}\,{\rm e}^{{\rm i}k\left(d_1+\frac{(x_1-\eta)^2}{2d_1}\right)}. \quad (2)$$

The analysis dealing with a point source can be easily extended to study the signal formation process of an arrayed source by performing an integration of the final intensity according to the source shape.

Assuming that the thickness of the sample along the optical axis is negligible compared to the focal length of the zone plate, the modulation of the x-ray wavefront after penetrating the sample with a refractive index $n=1-\delta+{\rm i}\beta$ is approximated by

$$U_1'(x_1,\eta) = U_1(x_1,\eta)\,{\rm e}^{-k\alpha(x_1)-{\rm i}k\phi(x_1)}, \quad (3)$$

where $\alpha(x_1)=\int\beta(x_1,z_1)\,{\rm d}z_1$ and $\phi(x_1)=\int\delta(x_1,z_1)\,{\rm d}z_1$ represent the decay and phase shift of the wave amplitude, respectively. Considering a pure phase object, i.e., $\alpha(x_1)=0$, its phase shift $\phi(x_1)$ is further supposed to be smooth, continuous and slowly varying. Hence, its derivative, essentially the angle of refraction, always exists. Based on these assumptions, the amplitude of the wave field in front of the zone plate becomes

$$U_2(x_2,\eta) = \mathscr{P}_{d_2}\left[U_1'(x_1,\eta)\right] \approx \frac{{\rm e}^{{\rm i}k\left(d_1+d_2+\frac{(x_2-\eta)^2}{2(d_1+d_2)}-\phi\left(\frac{\eta d_2+d_1x_2}{d_1+d_2}\right)\right)}}{\sqrt{{\rm i}\lambda\,(d_1+d_2)}}. \quad (4)$$

With the projection approximation, the wavefront after being modulated by the zone plate is written as

$$U_2'(x_2,\eta) = \sum_m \frac{V(x_2)}{\sqrt{|m|\pi}}\,{\rm e}^{\frac{-{\rm i}mkx_2^2}{2f}}U_2(x_2,\eta), \quad (5)$$

where $m=\pm1,\pm3,\ldots$, and f corresponds to the first order ($m=+1$) focal length of the zone plate. Note that the zero-order term corresponding to the transmission of the incident radiation in the forward direction is not included here. The reason is that such term would interfere with the imaging process involving the amplification by zone plate and is usually removed during experiments by a carefully designed imaging system.[10,14] The $V(x_2)$, closely related to the size of the zone plate, stands for the correction factor of its amplitude transmission function.[7] With an ideal zone plate having an infinitely large area, $V(x_2)$ becomes a constant ($V(x_2)=1$ is assumed) and the associated spatial resolution becomes infinitesimal.

Depending on the distance d_3, the complex amplitude of the x-ray wave field before the grating has two forms. If the grating is placed at the image plane of the source ($d_3=\frac{f(d_1+d_2)}{m(d_1+d_2)-f}$), the amplitude turns into an extreme value due to the use of the Dirac delta function at the beginning to simulate the point source. For the rest placement of the grating, the amplitude of the x-ray wave field is expressed by

$$\begin{aligned} U_3(x_3,\eta) &= \mathscr{P}_{d_3}\left[U_2'(x_2,\eta)\right] \\ &\approx \sum_m\sqrt{\frac{f}{{\rm i}\lambda\pi|m|q}}\,{\rm e}^{{\rm i}k\left(d_1+d_2+d_3+\frac{1}{2q^2}S(x_3,\eta)\right)}, \\ S(x_3,\eta) &= d_3\left(mx_3\left(d_1+d_2\right)+f(\eta-x_3)\right)^2 \\ &\quad +\left(d_1+d_2\right)\left(d_3\eta m+f(x_3-\eta)\right)^2 \\ &\quad -fm\left(d_3\eta+x_3\left(d_1+d_2\right)\right)^2 \\ &\quad -2q^2\phi\left(\frac{d_2\eta\left(f-d_3m\right)+d_3f\eta+d_1fx_3}{q}\right), \end{aligned} \quad (6)$$

where $q=d_3\left(f-m\left(d_1+d_2\right)\right)+f\left(d_1+d_2\right)$. In particular, the aforementioned x-ray microscope equipped with a Talbot (–Lau) interferometer[5,10] works under this condition.

The amplitude of the wavefront after the grating is obtained by the product of $U_3(x_3,\eta)$ and the periodic transmission function of the grating $T(x_3)$. Considering a 1D Ronchi grating with a duty cycle of 0.5, this equals to[15]

$$U_3'(x_3,\eta)=T(x_3)U_3(x_3,\eta)=\sum_{n=-\infty}^{\infty}a_n\mathrm{e}^{\frac{2in\pi x_3}{p}}U_3(x_3,\eta), \tag{7}$$

in which $T(x_3)$ is described by the form of Fourier series expansion, p represents the grating period, and the coefficient a_n is determined by the grating type and the diffraction order n.

The x-ray field reaching the detector plane is derived as

$$\begin{aligned}
U_4(x_4,\eta) &= \mathscr{P}_{d_4}\left[U_3'(x_3,\eta)\right]\approx\sum_{n=-\infty}^{\infty}\sum_m a_n\sqrt{\frac{f}{\mathrm{i}\lambda\pi|m|\tau}}\mathrm{e}^{\mathrm{i}k(d_1+d_2+d_3+d_4+Y(n,x_4,\eta))},\\
Y(n,x_4,\eta) &= -\frac{d_3}{2kp\tau}\left(4\pi(d_1+d_2)mnx_4-4\pi fnx_4+\eta^2kmp\right)-\phi\left(\frac{\eta kp\left(\tau-d_1\left(f-m(d_3+d_4)\right)\right)+d_1f\left(kpx_4-2\pi d_4n\right)}{kp\tau}\right)\\
&\quad-\frac{2\pi^2n^2d_4}{k^2p^2\tau}\left(d_3\left(f-(d_1+d_2)m\right)+(d_1+d_2)f\right)+\frac{f}{2\tau}(\eta-x_4)^2\\
&\quad-\frac{d_4\eta}{2kp\tau}(\eta kmp-4\pi fn)-\frac{x_4}{2kp\tau}(d_1+d_2)(kmpx_4-4\pi fn),
\end{aligned} \tag{8}$$

with $\tau=(d_1+d_2)(f-m(d_3+d_4))+(d_3+d_4)f$.

Further, the order m is set to $+1$ because the diffraction efficiencies of other odd orders decrease rapidly by a factor of $1/m^2$. Similarly, the diffraction order n of the grating is limited to 0 and ±1.[16] By the first-order approximation, the detected beam intensity, i.e., $|U_4(x_4,\eta)|^2$, is proportional to

$$\begin{aligned}
I(x_4,\eta) &\propto \frac{1}{2}+\frac{4}{\pi^2}+\frac{4}{\pi}\sin\left(\frac{\Theta_1+\Phi_1-\Theta_2-\Phi_2}{2}\right)\\
&\quad\times\cos\left(Cx_4+\frac{(\Theta_1+\Phi_1+\Theta_2+\Phi_2+\pi)}{2}\right),
\end{aligned} \tag{9}$$

where

$$\begin{aligned}
C&=\frac{2\pi}{pM}\left(1-\frac{d_3}{f}+\frac{d_4}{d_1M}\right),\\
\Theta_1&=-\frac{\pi d_4}{kp}C+\frac{2\pi d_4\eta}{d_1Mp},\\
\Theta_2&=\frac{\pi d_4}{kp}C+\frac{2\pi d_4\eta}{d_1Mp},\\
\Phi_1&=k\left(\phi\left(-\frac{kpx_4-2\pi d_4}{kpM}\right)-\phi\left(-\frac{x_4}{M}\right)\right),\\
\Phi_2&=k\left(\phi\left(-\frac{x_4}{M}\right)-\phi\left(-\frac{kpx_4+2\pi d_4}{kpM}\right)\right).
\end{aligned}$$

Introducing d_s as the distance between the zone plate and the image plane of the source ($d_s<d_3$ in our case), the expression of the factor C becomes

$$C=\frac{2\pi f(d_s-d_3)}{pM(d_2(f-d_s)+fd_s)}, \tag{10}$$

whose value is highly sensitive to the location of the grating. When the magnification M of the sample is sufficiently large, the object length d_2 approaches the focal length f, making the factor C become $\frac{2\pi(d_s-d_3)}{pMf}$. In addition, the period of the fringe pattern is equal to $2\pi/|C|$. And Θ_i $(i=1,2)$ denotes the constant phase shift. Without the sample, the fringe visibility is maximized when the absolute value of the sine term in Eq. (9) is equal to 1, which means that $d_4C=kpw/2$, $(w=\pm1,\pm3,\ldots)$. Solving this equation would generate the expression of $d_4\,(>0)$ as

$$d_4=\begin{cases}
\dfrac{Md_1f\left(M-\sqrt{\frac{2p^2w(d_1M+f)}{\lambda fd_1}+M^2}\right)}{2(d_1M+f)}, & 0>w\geq\frac{-M^2\lambda fd_1}{2p^2(d_1M+f)}, \quad (11a)\\
\dfrac{Md_1f\left(M+\sqrt{\frac{2p^2w(d_1M+f)}{\lambda fd_1}+M^2}\right)}{2(d_1M+f)}, & w\geq\frac{-M^2\lambda fd_1}{2p^2(d_1M+f)}. \quad (11b)
\end{cases}$$

Equations (11a) and (11b) represent different cases where the phase grating is close to or far from the detector, respectively.

To extract the phase information, the phase stepping (PS) approach is used. In practice, the grating is translated multiple times (denoted as an integer $M_{\mathrm{ps}}\geq3$) in the lateral direction by a certain distance Δ_{ps}. This operation can be theoretically described by replacing $T(x_3)$ in Eq. (7) with $T\left(x_3-\Delta_{\mathrm{ps}}\right)$. After repeating the same procedure from Eq. (7) to Eq. (9), the final intensity has a format of

$$\begin{aligned}
&I_{\mathrm{ps}}^{(j)}(x_4,\eta)\\
&\propto\frac{1}{2}+\frac{4}{\pi^2}+\frac{4}{\pi}\sin\left(\frac{\Theta_1+\Phi_1-\Theta_2-\Phi_2}{2}\right)\\
&\quad\times\cos\left(\frac{2\pi j}{M_{\mathrm{ps}}}+Cx_4+\frac{(\Theta_1+\Phi_1+\Theta_2+\Phi_2+\pi)}{2}\right),
\end{aligned} \tag{12}$$

where $\Delta_{\mathrm{ps}}M_{\mathrm{ps}}=p$ and $j=1,2,\ldots,M_{\mathrm{ps}}$. Normally the detected intensity forms a sinusoidal curve called as the phase stepping curve, from which the phase shift can be calculated analyti-

cally,

$$\frac{1}{2}\left(\Phi_1+\Phi_2+\Delta(x_4)\right)=\tan^{-1}\left[\frac{\sum_{j=1}^{M_{\rm ps}} I^{(j)}\sin\left(\frac{2\pi j}{M_{\rm ps}}\right)}{\sum_{j=1}^{M_{\rm ps}} I^{(j)}\cos\left(\frac{2\pi j}{M_{\rm ps}}\right)}\right], \quad (13)$$

in which $\Delta(x_4)=2Cx_4+\Theta_1+\Theta_2+\pi$ corresponds to the background measurement without the sample. Finally, the extracted phase signal is

$$\frac{\Phi_1+\Phi_2}{2}=\frac{k}{2}\left(\phi\left(-\frac{x_4}{M}+\frac{\lambda d_4}{pM}\right)-\phi\left(-\frac{x_4}{M}-\frac{\lambda d_4}{pM}\right)\right), \quad (14)$$

which is formally consistent with the derivations reported in Refs. [6,7]. It can be learned from this equation that the phenomenon of twin phase images would show up. These two enlarged (by a factor of M) phase images, split by a distance of $\frac{2\lambda d_4}{pM}$ from each other, have opposite amplitudes. And the magnitude of such positive and negative phase signals are reduced by 50%. If such separation becomes small enough compared with the resolution of the system ε, such phase difference signals would be converted into the differential phase signal, namely,

$$\frac{\Phi_1+\Phi_2}{2}\xrightarrow{\frac{\lambda d_4}{pM}<\varepsilon}\frac{\lambda d_4}{pM}k\phi'\left(-\frac{x_4}{M}\right). \quad (15)$$

Note that the sensitivity $\mathcal{S}$ of the DPI signal is represented by the coefficient of ϕ',

$$\mathcal{S}=\frac{2\pi d_4}{pM}. \quad (16)$$

On the premise of the optimal fringe visibility, it can be seen by substituting here the results of Eq. (11) that the value of sensitivity is determined by multiple imaging parameters and needs to be analyzed and optimized in combination with specific application scenarios. According to Eq. (15), there is always a competition between the separation and the sensitivity in realizing DPI since both of them are determined by the same factor of $\frac{\lambda d_4}{pM}$. Generally speaking, for a certain system resolution, the imaging system is more likely to operate in the DPI mode when the position of the phase grating d_4 satisfies the condition described by Eq. (11a).

Upon Eq. (9), the beam intensity of a microscopic imaging system with a Lau interferometer[12] or any other shaped source can be estimated by the integration of $I(x_4,\eta)$ on η. Considering a periodic x-ray source shown in Fig. 1, its intensity distribution follows the function[17]

$$\Gamma(\eta)=\begin{cases}1, & \ell p_0\le\eta<\left(\ell+\frac{1}{2}\right)p_0,\\ 0, & \left(\ell+\frac{1}{2}\right)p_0\le\eta<(\ell+1)\,p_0,\end{cases}$$
$$\ell=0,\pm1,\pm2,\ldots \quad (17)$$

The corresponding final detected intensity can be derived as

$$I(x_4)=\int\Gamma(\eta)I(x_4,\eta)\,\mathrm{d}\eta\propto\sum_{\ell=-\infty}^{\infty}\left(\frac{1}{4}+\frac{2}{\pi^2}\right)p_0$$
$$+\cos\left(Cx_4+\frac{(\Phi_1+\Phi_2+\pi)}{2}+\frac{\pi d_4 p_0}{d_1 Mp}\left(2\ell+\frac{1}{2}\right)\right)$$
$$\times\frac{4d_1Mp}{\pi^2 d_4}\sin\left(\frac{\pi d_4 p_0}{2Mpd_1}\right)\sin\left(\frac{\Phi_1-\Phi_2}{2}-\frac{\pi d_4}{kp}C\right),$$
$$\ell\in\mathbb{Z}. \quad (18)$$

Compared with Eq. (9), the main difference embodies in the fringe visibility when dealing with an arrayed x-ray source. To achieve a higher visibility, certain values of the period of the source are required. A quick estimate would be $p_0=\frac{Mpd_1}{d_4}\zeta$, $(\zeta=1,3,5,\ldots)$. When $\zeta=1$, the resulting values are found to be consistent with the grating periods reported in Ref. [10]. Note that such conclusion may need to be altered when the shape of the arrayed source varies. Nonetheless, similar results can be obtained by repeating the analysis procedure from Eq. (12) to Eq. (15). It was found that the period of the fringe and the separation of the twin phase images defined in Eq. (14) are independent to the shape of the source. This indicates that the proposed theoretical work can be used to predict the imaging condition for either PDI or DPI in an x-ray microscopy system integrated with a Talbot interferometer or a Lau one.

3. Numerical simulation

A series of 2D numerical simulations regarding the x-ray microscopic system shown in Fig. 1 are conducted. There comes with two main objectives. One is to verify the above theoretical derivations in comparison with the experimental measurements.[10,11] The other is to investigate the conversion condition and relationship between PDI and DPI. As discussed above, since the shape of the source only affects the fringe visibility, a point source is always considered in the subsequent numerical calculations for simplicity.

The subsequent simulation work is based on the previous theoretical derivation. Specifically, the Fresnel diffraction integral was calculated based on the discrete fast Fourier transform (DFFT) in Python. The transmission of x-rays through the optical components and the sample is imitated with the projection approximation. It is also assumed that the x-ray source is perfectly coherent and the detector has an ideal response without any crosstalk and photon shot noise. Besides, the resolution of the detector is determined by the discretization of the imaging field of view. To facilitate comparisons, the same imaging geometry and beam energy as listed in Ref. [10] were taken into account. In all simulations, the x-ray energy was fixed at 8.04 keV, and the imaging system ran in the large field of view (LFOV) mode with a 10-fold sample magnification. The simulated imaging field of view is 120 μm×120 μm with a zone plate having a resolution of 97.7 nm and a detector possessing a pixel dimension of 76.9 nm. Other key parameters to perform the calculations are shown in Table 1.

Table 1. Simulation parameters of the phase grating, zone plate and layout of the interferometer.

p (μm)	f (mm)	LFOV mode			
		d_1 (mm)	d_2 (mm)	d_3 (mm)	d_4 (mm)
2.4	61.9	68.7	68.0	132.6	559.0

The simulated fringe distribution without a sample is shown in Fig. 2(a). It has a period of 71.56 μm which can be obtained by Eq. (10). This is consistent with the value reported in Ref. [10]. The spatial resolution performance of the imaging system is evaluated in Fig. 2(b). The symmetrical structures in the figure are formed by overlapping two cylinders whose axes are parallel to the optical one. The offset distances associated with the three samples from left to right are 0.2 μm, 0.1 μm, and 0.0 μm, respectively. Due to the lens imaging procedure, an inverted image of the sample is found. The gray scale image shown here is actually the dark part of the phase difference image. Within it, the structure of 0.1 μm can hardly been seen since it is close to the resolution of the zone plate. In addition, the PDI results of different pure phase objects are displayed in Fig. 2(c). The sample contains two polystyrene spheres with diameters of 1.80 μm and 2.93 μm, and a rod of length 1.78 μm and diameter 1.27 μm. The corresponding maximum phase shifts for the Cu-$K\alpha$ x-ray photons are set to be 0.267 rad, 0.434 rad, and 0.662 rad, respectively. As shown in the bottom plot in Fig. 2(c), the simulated separation between the twin phase images (72.32 μm) and the extracted phase shift agree well with the experimental measurement in Ref. [11]. The minor oscillation remained on the curve is most likely caused by the discontinuity of the signal when performing the DFFT. These tests also serve as a supplement to the previous theory, which indicates that including a finite-size zone plate would not affect the theoretical findings in this work. Finally, the DPI results of the same sample are presented in Fig. 2(d). The grating period considered in this simulation is equal to 100 μm. As predicted by the theory, the resulting image is a DPI one. The discrepancy along the edge of the sample is due to the fact that the coefficient $\frac{\lambda d_4}{pM}$ cannot be infinitely small.

On the basis of Eq. (15), the inherent unity and conversion of the PDI and DPI are further demonstrated in Fig. 3. It is clear that certain imaging conditions involving the beam condition, imaging geometry (d_4/M), and the grating period are required in order to realize the PDI or DPI, provided that the system spatial resolution is pre-defined. In addition, the figure shows that the sensitivity of DPI increases as the grating period gets reduced or the spatial resolution decreases. Whereas, the sensitivity of DPI is enhanced with a larger value of d_4/M. The red colored boundaries (solid lines) in the two subplots are obtained by assuming that $\frac{\lambda d_4}{pM} = \varepsilon$. The boundaries would be shifted to the DPI side when $\frac{\lambda d_4}{pM} < \varepsilon$.

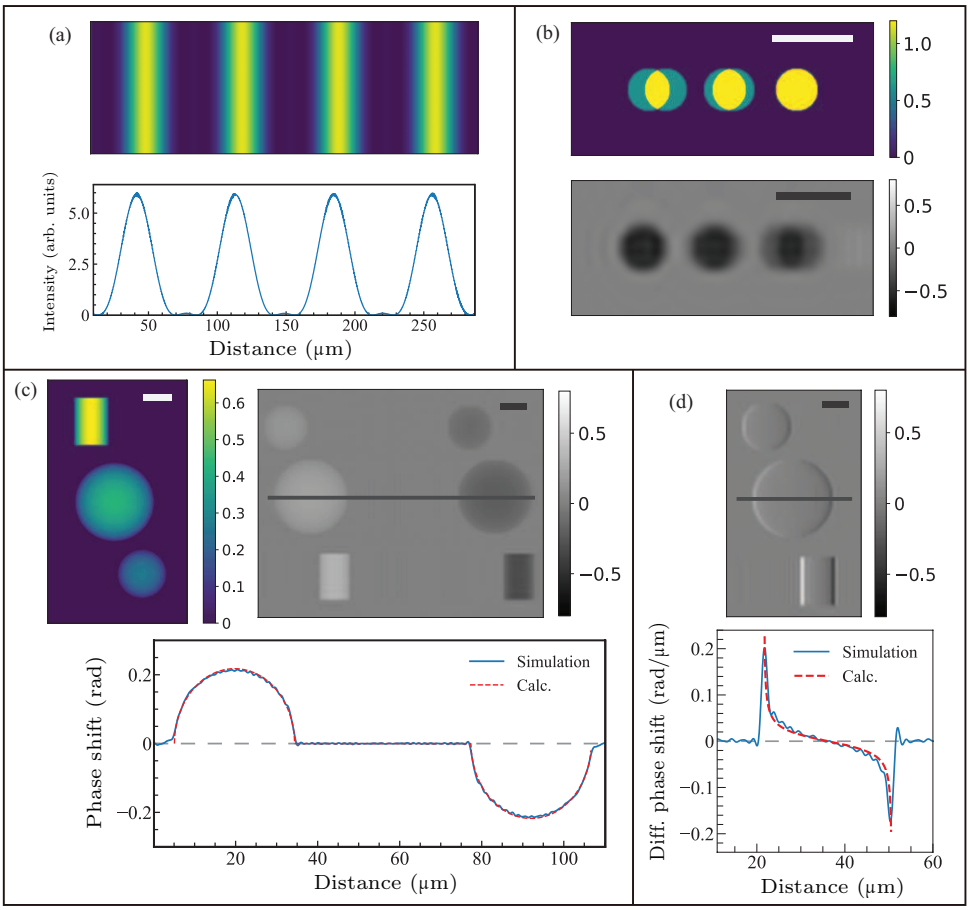


Fig. 2. Numerical simulation results: (a) the fringe distribution, (b) the phase difference imaging results to evaluate the spatial resolution, (c) the phase difference imaging results, and (d) the differential phase imaging results. The white and black scale bars denote 1 μm and 10 μm, respectively.

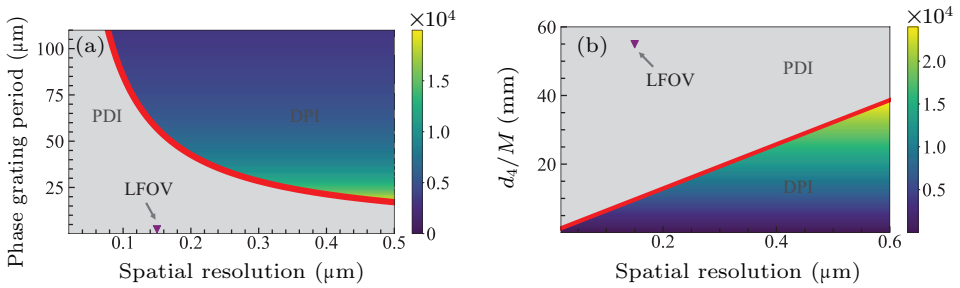


Fig. 3. Conversion conditions between PDI (gray area) and DPI (colored area) for the settings in Ref. [10]: (a) with varied spatial resolutions and grating periods; (b) with varied spatial resolutions and the geometrical factor d_4/M. The color bar denotes the sensitivity of the DPI. The inverted triangle corresponds to the LFOV mode.

4. Discussion and conclusion

As demonstrated in the theoretical analysis, both the PDI and the DPI can be explained by the same imaging theory, upon which the PDI and DPI are unified. Meanwhile, certain phase signals, either PDI or DPI ones, can be retrieved under specific imaging conditions. By adjusting the imaging condition appropriately, the PDI can be converted to the DPI, or vise versa. For instance, increasing the grating period while maintaining other system settings would transform the x-ray microscope from the PDI mode to the DPI mode. However, our theoretical analysis also reveals that the sensitivity of DPI may be limited when pursuing a high image resolution. To this end, the parameters of an x-ray microscope system integrated with a grating interferometer need to be carefully optimized to meet the desired imaging applications.

In conclusion, we have developed a comprehensive theoretical framework based on the diffraction theory to explain the formation of the phase information in a grating-based x-ray microscope. Analysis demonstrates that the phase difference imaging and the differential phase imaging originate from a unified phase imaging theory and can be converted by changing certain conditions. Additionally, the impact of different optical components including the x-ray source can be analyzed by this imaging theory. In future, optimizations such as exploiting different shaped and polychromatic x-ray sources and varied grating types would be investigated for given x-ray microscope imaging tasks.

Acknowledgements

Project supported by the National Natural Science Foundation of China (Grant Nos. 12027812 and 11804356) and the Youth Innovation Promotion Association of the Chinese Academy of Sciences (Grant No. 2021362).

References

[1] Momose A, Kawamoto S, Koyama I, Hamaishi Y, Takai H and Suzuki Y 2003 *Jpn. J. Appl. Phys.* **42** 866

[2] Pfeiffer F, Weitkamp T, Bunk O and David C 2006 *Nat. Phys.* **2** 258

[3] Shao Q, Chen J, Wali F, Bao Y, Wang Z, Zhu P, Tian Y and Gao K 2016 *Chin. Phys. B* **25** 108702

[4] Rong F, Gao Y, Guo C, Xu W and Xu W 2019 *Chin. Phys. B* **28** 108702

[5] Takeda Y, Yashiro W, Hattori T, Takeuchi A, Suzuki Y and Momose A 2008 *Appl. Phys. Express* **1** 117002

[6] Yashiro W, Takeda Y, Takeuchi A, Suzuki Y and Momose A 2009 *Phys. Rev. Lett.* **103** 180801

[7] Yashiro W, Harasse S, Takeuchi A, Suzuki Y and Momose A 2010 *Phys. Rev. A* **82** 043822

[8] Kuwabara H, Yashiro W, Harasse S, Mizutani H and Momose A 2011 *Appl. Phys. Express* **4** 062502

[9] Berujon S, Wang H, Pape I, Sawhney K, Rutishauser S and David C 2012 *Opt. Lett.* **37** 1622

[10] Takano H, Wu Y and Momose A 2017 *Developments in X-Ray Tomography XI*, September 26, 2017, San Diego, California, United States, p. 1039110

[11] Takano H, Wu Y, Irwin J, Maderych S, Leibowitz M, Tkachuk A, Kumar A, Hornberger B and Momose A 2018 *Appl. Phys. Lett.* **113** 063105

[12] Takano H, Hashimoto K, Nagatani Y, Irwin J, Omlor L, Kumar A, Tkachuk A, Wu Y and Momose A 2019 *Optica* **6** 1012

[13] Wolf A, Schuster M, Ludwig V, Anton G and Funk S 2020 *Opt. Express* **28** 13553

[14] Howells M, Jacobsen C, Warwick T and Van den Bos A 2007 *Science of Microscopy* (New York: Springer) pp. 835–926

[15] Liu X, Guo J, Peng X and Niu H 2007 *Chin. Phys.* **16** 1632

[16] Ge Y, Chen J, Zhu P, Yang J, Deng S, Shi W, Zhang K, Guo J, Zhang H, Zheng H and Liang D 2020 *Opt. Express* **28** 9786

[17] Wang Z, Zhou R, Zhao L, Ren K, Xu W, Liu B and Chen H 2021 *Chin. Phys. B* **30** 028702